# Probing the Flexibility of Internal Rotation in Silylated Phenols with the NMR Scalar Spin−Spin Coupling Constants

**Vladimír Sychrovský,*,† Ladislav Benda,† Alexandr Prokop,† Vratislav Blechta,‡ Jan Schraml,‡ and Vladimír Špirko†**

*Institute of Organic Chemistry and Biochemistry of the ASCR, v.v.i., Flemingovo sq. 2., 166 10 Prague 6, Czech Republic, and Institute of Chemical Process Fundamentals of the ASCR, v.v.i., Rozvojová 135, 165 02, Prague 6, Czech Republic*

*Received: December 17, 2007; Revised Manuscript Received: March 13, 2008*

The rotation of a trimethylsiloxy (TMSO) group in three silylated phenols (with three different *ortho* substituents −H, $-CH_3$, and $-C(CH_3)_3$) was studied with the NMR $^nJ$(Si,C), $n = 2, 3, 4, 5$, scalar spin−spin coupling between the $^{29}$Si nucleus of the TMSO group and the $^{13}$C nuclei of the phenyl ring. The internal rotation potential calculated with the B3LYP and MP2 calculation methods including the effect of a solvent environment (gas phase, chloroform, and water) was used for the calculation of the dynamical averages of the scalar coupling constants in the framework of the rigid-bender formalism. Solvent effects, the quality of the rotational potential, and the applicability of the classical molecular dynamic to the problem is discussed. Quantum effects have a sizable impact on scalar couplings, particularly for the internal rotational states well localized within the wells of the potential surfaces for the TMSO group. The overall difference between the experimental and theoretical scalar couplings calculated for the global energy-minima structures (static model) decreases substantially for both model potentials (B3LYP, MP2) when the molecular motion of the TMSO group is taken into account. The calculated data indicate that the inclusion of molecular motion is necessary for the accurate calculation of the scalar coupling constants and their reliable structural interpretation for any system which possesses a large-amplitude motion.

## Introduction

Nuclear magnetic resonance (NMR) has become an indispensable experimental technique for the determination of molecular structure and conformation.[1] Experimentalists and synthetic chemists can usually rely on empirical rules for the structural interpretation of NMR parameters.[2–7] In some cases, however, such an empirical approach may not be suitable, and the experimental values of NMR parameters cannot be straightforwardly related to the molecular structure. For example, the calculated effects of molecular vibrations on NMR shifts[8] and scalar couplings[9–11] were shown to be significant. From the theoretical point of view, it is always advisable to take vibrational behavior into account in order to ensure the plausibility of the predicted NMR parameters.[12] On the other hand, solving the vibrational problem itself may represent a nontrivial task. The theoretical methods for the calculation of the NMR properties that include polarization of the solute by solvent and the effect of molecular motion have recently been reviewed.[13]

This work focuses on the correlation of the measured NMR scalar couplings with the structural parameters of silylated phenols. The static approach is shown to be inadequate when accounting for the flexibility of the TMSO group in silylated phenols. The studied molecules were especially designed to allow a stepwise probing of the internal molecular rotation of the TMSO group. The internal rotation barrier of the TMSO group gradually increases when the *ortho* proton is replaced by the $-CH_3$ and $-C(CH_3)_3$ groups. The scalar coupling constants reflect different rotational flexibility as the spin−spin coupling pathway essentially coincides with the internal rotation coordinate. By including both the internal rotation and solvent effects into the theoretical model, we have calculated the scalar couplings probably at the accuracy that corresponds to the current limit achievable by means of the used ab initio methods.

**SCHEME 1: A schematic representation of the three substituted silylated phenols, R = H, $CH_3$, and $C(CH_3)_3$**

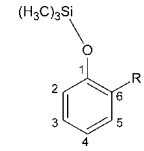


## Calculation Method

The molecular geometry was optimized using the B3LYP[14] and the MP2[15] methods. Single-point energy calculations were also performed with the CCSD method.[16,17] The basis set (4s,1p) → [2s,1p] for hydrogen,[18] (10s,4p,1d) → [3s,2p,1d] for carbon,[18] and (16s,10p,1d) → [4s,3p,1d] for silicon[19] called 6-31G(d, p) was used for the geometry optimization.

The potential energy surfaces were calculated as stepwise variations of the torsion angle (the torsion along the link atoms between the TMSO group and the phenyl ring, Scheme 1) while optimizing the rest of the geometry parameters. The actual calculations were performed for two solvents (chloroform and water), which were modeled using the polarizable continuum model[20] (PCM) as implemented in the Gaussian 03 program package.[21]

* To whom correspondence should be addressed. E-mail: vladimir.sychrovsky@uochb.cas.cz.
† Institute of Organic Chemistry and Biochemistry of the ASCR.
‡ Institute of Chemical Process Fundamentals of the ASCR.

10.1021/jp711809e CCC: $40.75 
Published on Web 05/20/2008

The NMR scalar spin−spin coupling constants[13,22] were calculated using the CP DFT method[23,24] with the B3LYP functional employing the atomic basis usually called IgloIII.[25] All four coupling terms were included, that is, the diamagnetic spin−orbit (DSO), paramagnetic spin−orbit (PSO), Fermi contact (FC), and spin dipolar (SD), thus yielding the total scalar coupling constant. The scalar couplings $^nJ(^{29}Si,^{13}C)$ were calculated for the pair of silicon and carbon atoms separated by $n$ bonds ($n$ = 2, 3, 4, 5). The PCM approach was used consistently in geometry optimization and the calculation of the scalar couplings.

All calculations were performed with the G03 program package.[21]

**Dynamical Calculations.** The dynamical calculations were performed within the framework of the rigid-bender formalism[26,27] using a nonrigid molecular reference closely following the internal rotation of the TMSO group with respect to the phenyl ring of the studied molecules (the motion being measured by $\tau$). The appropriate Hamiltonian acquires the following form

$$\hat{H} = 1/2\mu_{\tau\tau}\hat{J}^2{}_\tau + 1/2(\hat{J}_\tau\mu_{\tau\tau})\hat{J}_\tau + 1/2\mu^{1/4}\{\hat{J}_\tau\mu_{\tau\tau}\mu^{-1/2}[\hat{J}_\tau\mu^{1/4}]\} + V(\tau) \quad (1)$$

where $J_\tau = -i\beta(\mathrm{d}/\mathrm{d}\tau)$, $\mu_{\tau\tau}$ is the internal rotation component of the tensor, which is the inverse of the 4 × 4 generalized Hougen−Bunker−Johns[27] molecular inertia tensor, $\mu$ is the determinant of the matrix $[\mu_{\alpha\beta}]$ ($\alpha,\beta$ = $x,y,z$, $\tau$; $x,y,z$ being Cartesian atomic coordinates in the molecular-fixed-axis system), and $V(\tau)$ is the internal rotation (energy minimum path) potential (for further details, see refs 26 and 27).

Effective, state-dependent spin−spin coupling constants $^nJ(\mathrm{Si,C})(i)$ are evaluated as the following averages[28,29]

$$^nJ(\mathrm{Si,C})(i) = \langle\psi_i(\tau)|J(\mathrm{Si,C})(\tau)|\psi_i(\tau)\rangle \quad (2)$$

where $\Psi_i(\tau)$ is the wave function of a given internal rotation state $i$.

To allow for a qualitative estimation of the temperature dependence of the probed coupling constants, the following thermal average characteristics are also evaluated

$$\langle J(\mathrm{Si,C})\rangle_T = \Sigma_j J(\mathrm{Si,C})(j)\exp\{-E_j/kT\}/\Sigma_j\exp\{-E_j/kT\} \quad (3)$$

where $E_j$ are internal rotation energies, $T$ is temperature, and $k$ is the Boltzmann constant.

Making it possible for the molecular valence coordinates to vary with the "low-frequency" internal rotation coordinate $\tau$, the model allows for the important interactions with the remaining "high-frequency" molecular vibrational modes (see, e.g., ref 30). As a matter of fact, these adiabatically accounted interactions are of only minor consequences, thus evidencing the rather marginal role of the remaining (high-frequency) molecular vibrations in the dynamical averaging.

**Classical MD Simulation.** The dynamical behavior of silylated phenol with an *ortho* proton was probed using a MD simulation technique with the program TINK[31] and the Universal Force Field[32] employing an implicit chloroform solvent at room temperature (300 K). The classical internal rotation potential function was replaced by the potential function calculated with the B3LYP method employing the PCM chloroform solvent. The snapshot geometries (54 geometries) along the trajectory sampling the internal rotation coordinate were randomly selected and, in turn, used for the calculation of the scalar couplings.

## Experimental Section

**Synthesis.** The studied compounds were prepared by means of standard synthetic methods; the details will be published elsewhere.[33]

**NMR Measurements.** $^{13}C$ and $^{29}Si$ NMR spectral measurements in solution were performed on a Varian UNITY-500 spectrometer (operating at 499.9 MHz for $^1H$, at 125.7 MHz for $^{13}C$, and at 99.3 MHz for $^{29}Si$ NMR measurements) using a 5 mm Si{C,H} Nalorac probe. The spectrometer was equipped with an X,Y,Z-Performa gradient module and has four rf channels, two of which were fitted with waveform generators. The standard vnmr 6.1C software was used for all of the experiments except for the (Si,C,Si)gHMQC pulse sequence. All of the spectra were recorded at 25 °C in 0.3−1.5 M solutions in dry $CDCl_3$ (Aldrich, 99.8 atom % D, stored over activated molecular sieve 3A) containing 1% (v/v) of hexamethyldisilane (Aldrich, HMDSS, $^{29}Si$ secondary reference). The $^{13}C$ NMR spectra were measured using a spectral width of 30 000 Hz. The WALTZ decoupling was applied during both the acquisition (1 s) and relaxation delay (10 s). Zero filling to 128K and a mild line broadening were used in data processing. The spectra were referenced to the line of the solvent ($CDCl_3$, $\delta$ = 76.99 ppm). The $^{29}Si$ NMR spectra were measured by the INEPT pulse sequence as modified for $Si(CH_3)_3$ groups[34] (75 ms polarization and 16 ms refocusing delays optimized for polarization transfer by $^2J(^{29}Si-C-^1H)$ = 6.7 Hz from a nine-spin proton system) using a relaxation delay of 10 s, a spectral width of 10 000 Hz, an acquisition time of 4 s, and FID data zero filled to 128K. The spectra were referenced to the line of HMDSS ($\delta$ = −19.79 ppm).

The (Si,C,Si)gHMQC correlation experiment employed the pulse sequence described earlier,[35] with the INEPT part the same as that described above for the INEPT experiment. Each sample was measured with two values of polarization transfer delay (Si → C) in the gHMQC part of the sequence, 160 and 500 ms. The former value was used in measurements of the couplings in the 1−3 Hz range, and the latter was for the couplings below 1 Hz. The intensity of the first gradient pulse was 9.93 gauss·cm$^{-1}$, whereas that of the second alternated between 2.74 and −22.5 gauss·cm$^{-1}$ for the two FIDs needed for phase-sensitive 2D detection. The 90° pulses of $^1H$, $^{13}C$, and $^{29}Si$ were 18, 20, and 8 $\mu$s long, respectively. The other parameters were set at an acquisition time of 4.0 s, a spectral width in the F2 ($^{29}Si$) dimension of 2000 Hz with zero filling to 64K data points and a Gaussian broadening (5 s), a relaxation delay of 10 s, a gradient duration of 1 ms, and a spectrometer recovery time of 1 ms. The spectral width in the F1 dimension was 6000 Hz, at 2 × 32 t1 increments, at least 16 scans per increment, zero filling to 256 and a Gaussian broadening (0.005 s).

It is not problematic to achieve a line width of 0.1 Hz or even less when a sufficiently long acquisition time is used in the measurements of these samples by the standard refocused decoupled INEPT[34,36] and with sufficient digitalization to measure the peak position within an accuracy of 0.02 Hz. In the measurements reported here, a shorter acquisition time had to be used in order to avoid the occurrence of echoes during the detection period and to get a sufficient *S*/*N* ratio in a reasonable time.

In the (Si, C,Si)gHMQC spectra, the coupling constants are read off from the separations of lines in the antiphase doublets along the F2 axis. In determining the coupling constants in the range of 1−3 Hz (measured with a polarization delay of 160 ms), no overlap occurred, and the antiphase lines were well separated by a plateau and allowed measurements of the line widths (at half-height) that were subsequently used in line simulations for small couplings. The observed small separations that were measured with a delay of 500 ms were corrected by simulations to yield estimates of the coupling constants. The

corrections varied between 0.00 and 0.10 Hz for the couplings of 0.60 Hz or less, depending on the separation and line width determined from those experiments employing a shorter delay. Although the antiphase line separation could be read with a precision of ±0.04 Hz, the accuracy of the corrected values was estimated as asymmetrical within −0.10 and +0.05 Hz.

The unambiguous and independent assignments of the lines in the $^{13}C$ NMR spectra (based on $^{13}C$ line intensity, multiplicity, and $^{1}H-^{13}C$ correlations) will be described elsewhere.[33]

## Results and Discussion

**Rotation of the Trimethylsiloxy Group.** The internal rotational barrier of the TMSO group is affected specifically by the group in the *ortho* position of the phenyl ring (Scheme 1). If there is only a hydrogen atom in the *ortho* position, the TMSO group can rotate, nearly freely, around the O−C1 bond (the calculated B3LYP barrier is 0.5 kcal/mol, Figure 1). If there is a larger *ortho* substituent (R = $CH_3$, R = $C(CH_3)_3$), the rotation is hindered effectively, and the potential energy increases steeply when the value of the torsion angle Si−O−C1−C6 (further called torsion $\tau$) approaches the interval of 0−90°, which corresponds to a steric clash between the TMSO group and the substituted group (Figure 1). The two kinds of molecular motion (free and hindered) of the TMSO group were described at the B3LYP and MP2 levels of theory. The free rotation was also modeled using the classical molecular dynamic (MD) simulation technique.

The optimal values of $\tau$ calculated for the global energy minimum with the B3LYP method including a chloroform solvent (B3LYP(chloroform)) were 90, 114, and 164° for the substituents −H, $-CH_3$, and $-C(CH_3)_3$, respectively. The more the rotational coordinate $\tau$ is confined in space due to the increasing size of the *ortho* substitution, the more the optimal value is shifted toward the antiperiplanar orientation with respect to carbon C6 (Scheme 1). The geometries optimized with the B3LYP and MP2 methods were not the same. The optimal torsion angles $\tau$ calculated with the MP2(chloroform) method were 90, 108, and 134° for the −H, $-CH_3$, and $-C(CH_3)_3$ substitution, respectively. The value of the bond angle Si−O−C1 calculated with the B3LYP method was larger than the angle calculated with the MP2 method for the same geometry grid point. For example, the Si−O−C1 angles calculated with the B3LYP(chloroform) and MP2(chloroform) method (R = H; $\tau$ = 90°) were 126 and 120°, respectively. The MP2 geometries thus possess a closer spatial proximity of the TMSO group and phenyl ring.

The B3LYP and MP2 calculation methods also provide different internal rotation potentials. Consequently, the corresponding internal rotation wave functions and thus also the NMR parameter averages differ for these methods, as will be shown further.

The location of the TMSO group above the phenyl ring (R = H; $\tau \sim 45-135°$; Figure 2) leads to a drop in the potential energy. The MP2 potential curve drops roughly four times more sharply than the B3LYP one (Figure 2). The same trend (i.e., a larger decrease for the MP2 method) was also predicted for the hindered rotation potential ($\tau$ between the global minima and 180°; R = $CH_3$, R = $C(CH_3)_3$; Figure 3). Once the TMSO group gets close to the *ortho* group, both potentials become closer (Figure 3).

The calculated potential energy surfaces (R = H; B3LYP and MP2) differ qualitatively. Whereas the B3LYP curves possess one global ($\tau$ = 90°) and one local ($\tau$ = 0°) minimum, the MP2 curves exhibit only one global minimum ($\tau$ = 90°)

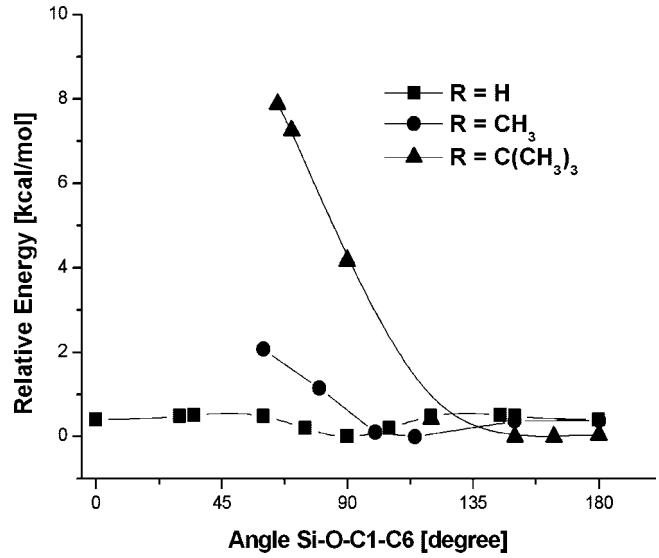


**Figure 1.** The dependence of energy on the rotation of the TMSO group relative to the energy of the global minimum calculated with the B3LYP method and a chloroform solvent.

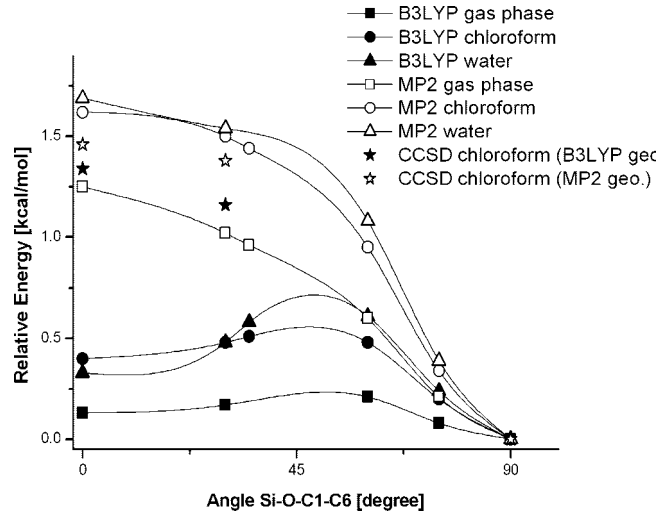


**Figure 2.** The dependence of energy on the rotation of the TMSO group relative to the energy of the global minimum calculated for the R = H substitution.

with the maximum of the rotation barrier at $\tau$ equal to 0° (Figure 2). The energy difference between the local and global minima calculated with the B3LYP(chloroform) method is only 0.4 kcal/mol, while the MP2(chloroform) barrier is 1.6 kcal/mol (Figure 2).

The quantum description of the internal rotation states is strongly affected by the shape of the calculated potential energy curve (R = H; B3LYP, MP2; Figure 4). Whereas the low-lying rotational states are localized in the region of the global energy minimum for both potentials ($\tau$ = 90°; Figure 4), some higher states calculated with the B3LYP potential ($i$ = 16, 17,. . ., 30 and $i$ = 31, 32, 33) are localized in the region of local minima ($\tau$ = 0, 180°; Figure 4). Localization of the quantum states (calculated as a maximum of the square of the rotational wave function) modeled with the B3LYP potential alternates between the global and local minima. On the other hand, the MP2 rotational states are well localized in the global minimum region for all states lying below the MP2 rotation barrier (Figure 4). The states lying safely above the barrier ("free rotation" states) are delocalized over the whole space. Since the global minimum

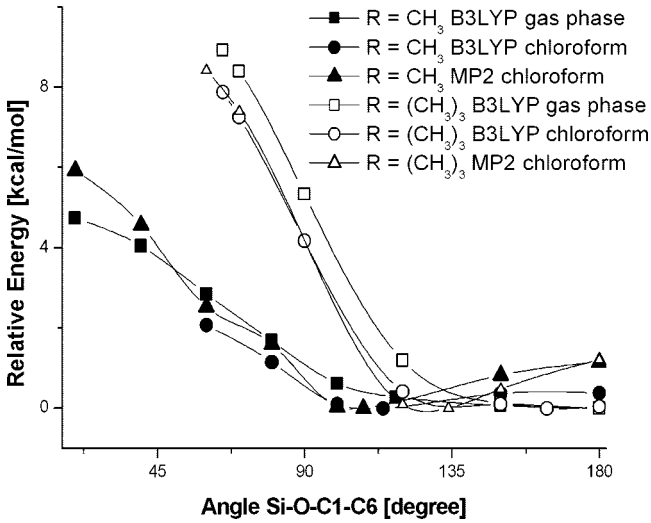


**Figure 3.** The dependence of energy on the rotation of the TMSO group relative to the energy of the global minimum calculated for the substitutions R = $CH_3$ and R = $C(CH_3)_3$.

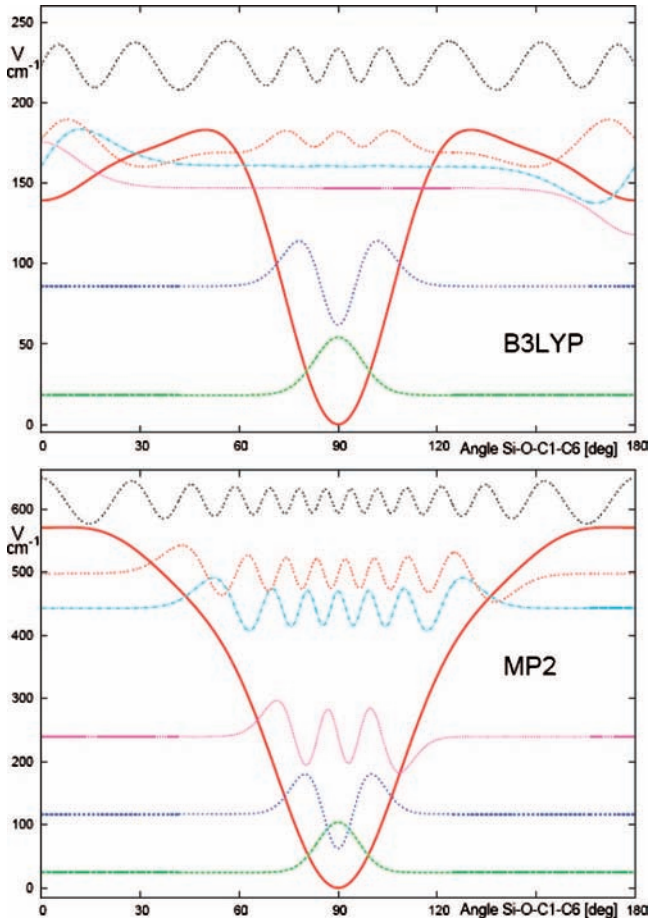


**Figure 4.** The B3LYP and MP2 rotation potentials (thick lines) and wave functions of some localized, nearly delocalized, and completely delocalized internal rotation states calculated for the TMSO group. The energies of the rotational states in $cm^{-1}$ are represented by the baselines of the plotted wave functions.

of the MP2 surface is deeper than the B3LYP one, the delocalization of the MP2 states requires higher activation energy.

The potentials calculated for the hindered rotation possess only one global minimum (Figure 3). The rotation of the TMSO group is spatially confined by an effectively infinite barrier (R = $CH_3$, R = $C(CH_3)_3$; Figure 3). All quantum internal rotational states are thus localized within the interval confined by the steric clash, and the spreading of their wave functions increases as the activation energy increases.

**Effect of Solvent on the Rotation Potential.** A solvent environment affects the calculated profile of the rotational potentials for both kinds of rotational motions (Figures 2 and 3). Three environments with an increasing polarity of solvent (gas phase, chloroform, and water) were considered. The gas-phase calculation and inclusion of the PCM water solvent theoretically mimic the limit conditions with regard to the experiment (chloroform). (The NMR experiment using water solvent is only hypothetical as moisture leads to a decomposition of the compounds.)

A relatively large solvent effect, up to ~0.3 kcal/mol, was calculated for the internal rotation potential of the TMSO group without steric hindrance (R = H; Figure 2). The separation between the curves calculated in the gas phase and chloroform is comparable for both methods used (Figure 2). The additional increase of the polarity of the solvent (water) has only a marginal effect on the calculated potential (chloroform), increasing the energy near the global minima and decreasing the energy in the region of the antiperiplanar arrangement (Figure 2). The separation of the potential curves calculated for chloroform and water is smaller than 0.1 kcal/mol (Figure 2). The effect of polarization of the solute by the solvent on the internal rotation potential is thus already saturated for chloroform, and the impact of the calculation method (B3LYP, MP2) dominates (Figure 2).

The same effect of solvent (increase in energy) on the rotation potential as that calculated for the free rotation (R = H) was also found for the hindered rotation when the TMSO group was spatially well separated from the substituent (the region between the global energy minimum and antiperiplanar arrangement; Figure 3). An opposite trend, a decrease in energy due to the solvent effect, was found for the area of steric clash (Figure 3). The separation of the B3LYP potential curves in the gas phase and chloroform was smaller than 0.5 for R = $CH_3$ and 0.1 kcal/mol for R = $C(CH_3)_3$ (Figure 3).

The rotational flexibility of the TMSO group was respected using the classical molecular dynamic (MD) simulation only for the free rotation (R = H). The dispersion of the calculated energies was much larger ($\Delta E \sim 14$ kcal/mol; 54 selected MD geometries; NMR calculation; see Supporting Information) than the barrier ($\Delta E \sim 0.5$ kcal/mol; Figure 1) obtained using the B3LYP(chloroform) method. This is because of the inclusion of all of the vibration modes in the MD calculation; the rotation of the TMSO group is only one of many molecular motions. The calculated energies ($\Delta E \sim 14$ kcal/mol) therefore do not exhibit any smooth dependence on the rotation coordinate. We note that the MD geometries calculated using the universal force field[31,32] differ qualitatively from the B3LYP and MP2 grid point geometries. This difference may result in systematic shifts of the NMR parameters, as will be shown in the next section.

**Quality of the Potential for the Internal Rotation.** The choice of the quantum chemical method used for the calculation of the internal rotation potential of the TMSO group obviously affects the rotational barrier and curvature of the calculated potential surfaces (Figures 2 and 3). The interaction between the phenyl aromatic ring and the methyl group(s) is clearly different when described with the B3LYP or MP2 method. The trends calculated for the internal rotation in the silylated phenols are in agreement with the recent calculation carried out also with the B3LYP and MP2 methods in peptides containing an

**TABLE 1: The Scalar Spin−Spin Coupling Constants between a $^{29}$Si Atom of the Trimethylsilyl Group and a $^{13}$C Carbon of the Phenyl Ring in the Three Silylated Phenols[a]**

| substitution[b] | method[c] | $^2J$(Si,C$_1$) | $^3J$(Si,C$_2$) | $^3J$(Si,C$_6$) | $^4J$(Si,C$_3$) | $^4J$(Si,C$_5$) | $^5J$(Si,C$_4$) |
|---|---|---|---|---|---|---|---|
| R = H | static | −2.92/−2.74 | 1.04/1.12 | 1.04/1.12 | −0.80/−0.89 | −0.80/−0.89 | 0.80/0.89 |
| | $\langle J\rangle_{55/120}$ | −2.60/−2.46 | 2.14/2.37 | 2.14/2.37 | −0.16/−0.10 | −0.16/−0.10 | 0.32/0.31 |
| | $\langle J\rangle_{T=293K}$ | −2.66/−2.63 | 1.95/1.52 | 1.95/1.52 | −0.28/−0.62 | −0.28/−0.62 | 0.40/0.69 |
| | MD−DFT | −1.17 | 2.40 | 2.4 | −0.60 | −0.60 | 0.78 |
| | experiment[d] | −2.08 | 1.67 | 1.67 | −0.33 | −0.33 | 0.42 |
| R = $CH_3$ | static | −2.87/−2.71 | 1.04/1.14 | 1.72/1.51 | −0.47/−0.68 | −0.67/−0.80 | 0.64/0.78 |
| | $\langle J\rangle_{55/80}$ | −2.9/−2.7 | 1.4/1.7 | 1.9/2.2 | −0.3/−0.3 | −0.5/−0.5 | 0.5/0.5 |
| | $\langle J\rangle_{T=293K}$ | −2.7/−2.6 | 1.5/1.5 | 2.6/2.1 | 0.1/−0.6 | −0.4/−0.4 | 0.3/0.6 |
| | sxperiment[d] | −2.12 | 1.28 | 1.95 | −0.49 | −0.25 | 0.43 |
| R = $C(CH_3)_3$ | static | −2.68/−2.46 | 2.34/1.86 | 3.27/2.36 | 0.34/−0.07 | 0.52/−0.34 | 0.02/0.37 |
| | $\langle J\rangle_{55/80}$ | −2.9/−2.9 | 1.5/1.7 | 2.2/1.9 | −0.4/−0.3 | −0.1/−0.5 | 0.4/0.5 |
| | $\langle J\rangle_{T=293K}$ | −2.7/−2.5 | 2.1/2.1 | 2.9/2.6 | −0.1/0.1 | 0.3/−0.2 | 0.1/0.3 |
| | experiment[d] | −1.95 | 1.83 | 2.69 | −0.20 | −0.25 | 0.25 |

[a] The scalar couplings in Hz. [b] See Scheme 1. [c] Static (B3LYP/MP2) is a NMR calculation for the B3LYP and MP2 equilibrium geometry including a chloroform solvent. $\langle J\rangle_{n/m}$ is the average coupling for individual rotational states $n$ and $m$ calculated using the B3LYP and MP2 potential, respectively. $\langle J\rangle_{T=293K}$ (B3LYP/MP2) is a thermal average calculated with the B3LYP and MP2 rotational potential. [d] The signs were not measured.

aromatic ring.[37] In particular, the dispersion interaction is known to be inadequately described by the B3LYP method, leading thus to the underestimation of the stabilization energy,[38,39] while application of the MP2 method leads to the relative increase of the stabilization energy.[40] In order to assess the reliability of both model potentials, we carried out the single-point CCSD energy calculations ($\tau$ = 0, 30, 90°; Figure 2) for the grid point geometries optimized with the B3LYP and MP2 methods including chloroform solvent. As the dispersion contribution is treated more properly with the CCSD method, notable increase of the rotational barrier for the grid point geometries optimized with the B3LYP method was obtained (Figure 2). On the other hand, for the grid point geometries optimized with the MP2 method, a relative decrease in energy was calculated. Both CCSD grid point calculations thus give the rotational barriers that are confined between the potential curves obtained with the MP2 method in the gas phase and chloroform, which gives somewhat higher credibility to the MP2 potential compared to the B3LYP one.

**Calculation of the NMR Spin−Spin Coupling Constants.** The scalar coupling constants were calculated for the silicon nucleus of the TMSO group and the inner ring carbon nuclei of the phenyl ring in the three silylated phenols (Scheme 1). The absolute magnitudes of the calculated couplings range from 2.7 ($^3J$(Si,C)) to 0.2 Hz ($^nJ$(Si,C), $n$ = 4, 5), in agreement with the measured couplings (Table 1). The calculation predicts a negative sign for the $^nJ$(Si,C), $n$ = 2, 4, coupling constants, whereas the opposite sign is calculated for an odd number of bonds ($n$ = 3, 5) separating the coupled nuclei. The sign of the couplings has not been determined experimentally yet.

The symmetrically disposed carbon atoms in pairs (C2,C6) and (C3,C5) are indistinguishable in the NMR experiment only for the compound with R = H. In this case, the dependence of the $^3J$(Si,C) and $^4J$(Si,C) couplings on the torsion angle $\tau$ was averaged ($^nJ$(Si,C) = 1/2($^nJ$(Si,C′) + $^nJ$(Si,C″)), $n$ = 3, 4; (C′,C″) was (C2,C6) or (C3,C5)).

The geometry optimization and NMR calculations were performed using the same solvent model. As the NMR calculations were performed only with the B3LYP method, the "MP2 scalar couplings" will hereafter refer to the NMR calculation carried out with the B3LYP method using the geometry optimized with the MP2 method.

The values of the scalar couplings calculated for different environments are very similar. The choice of the method for geometry optimization has a greater impact on the calculated couplings than the model of solvent. The difference between the couplings calculated with the B3LYP method in the gas phase and those in chloroform is smaller than 0.1 Hz, and a similar shift was calculated also for water (Supporting Information). The difference between the scalar couplings calculated using the B3LYP and MP2 geometries in chloroform was smaller than 0.2 and 0.8 Hz for the free (R = H) and hindered rotation (R = $CH_3$, $C(CH_3)_3$), respectively.

If the rotation freedom of the TMSO group is large, both the geometry and solvent effects are comparable. For example, the $^2J$(Si,C1) coupling calculated with the B3LYP method in the gas phase, chloroform, and water (R = H; $\tau$ = 90°) is −2.92, −2.92, −2.93 Hz, respectively. For the geometry optimized with the MP2 method, the $^2J$(Si,C1) coupling is −2.76, −2.74, −2.72 Hz, respectively. The B3LYP and MP2 couplings differ more profoundly for geometries in the region of steric clash (Supporting Information).

Substitution at the *ortho* carbon has a specific effect on the calculated scalar couplings $^nJ$(Si,C), $n$ = 2, 3, 4, 5 (B3LYP(chloroform); Figures 5–8). The curves for the individual couplings calculated for the discussed substitutions do not coincide (Figures 5–7), with the exception of the $^5J$(Si,C4) coupling (Figure 8). The calculated dependence of the $^5J$(Si,C4) couplings on the torsion $\tau$ is therefore not affected by the *ortho* substitution (B3LYP, Figure 8, and also MP2, Supporting Information). The measured values of the $^5J$(Si,C4) coupling are 0.42, 0.43 and 0.25 Hz for the −H, $-CH_3$, and $-C(CH_3)_3$ group, respectively. This observed decrease (Table 1) agrees with the prediction obtained with the "static" approach, because the optimum for the torsion $\tau$ shifts toward the antiperiplanar arrangement due to the size of the substituted group (B3LYP, $\tau$ = 90, 114, 164°, and MP2, $\tau$ = 90, 108, 134°).

The absolute difference between the calculated (static approach; Table 1) and measured couplings ranges from 0.8 ($^2J$(Si,C1); R = H; B3LYP) to 0.0 Hz ($^4J$(Si,C3); R = $CH_3$; B3LYP). The averages of the absolute difference of the calculated couplings from the experiment were 0.6/0.6, 0.3/0.4, and 0.6/0.2 Hz (B3LYP/MP2) for the substitutions R = H, R = $CH_3$, and R = $C(CH_3)_3$ (static approach; Table 1).

The internal rotation wave functions calculated for the TMSO group (Figure 4) were used for the calculation of the average scalar couplings (eqs 2 and 3 in the Dynamical Calculations subsection). The averages were calculated for the individual

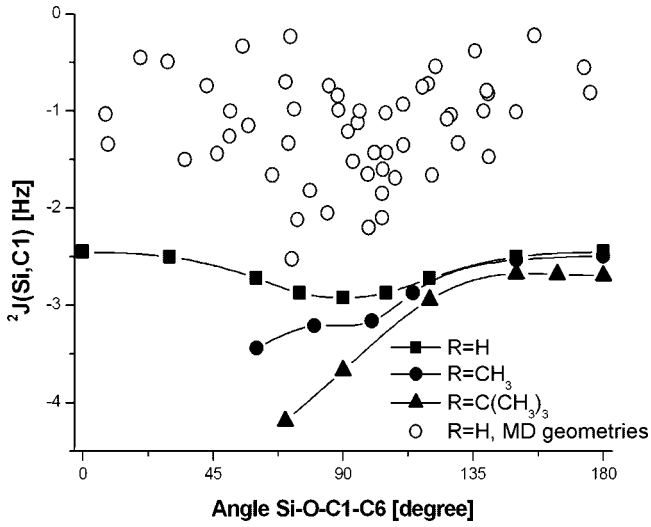


**Figure 5.** The dependence of the $^2J$(Si,C2) coupling on the rotation of the TMSO group calculated with the B3LYP method including a chloroform solvent.

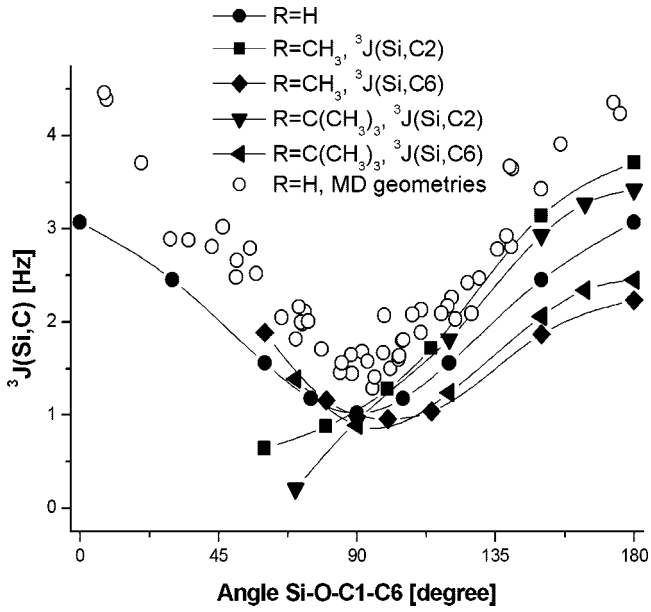


**Figure 6.** The dependence of the $^3J$(Si,C) couplings on the rotation of the TMSO group calculated with the B3LYP method including a chloroform solvent.

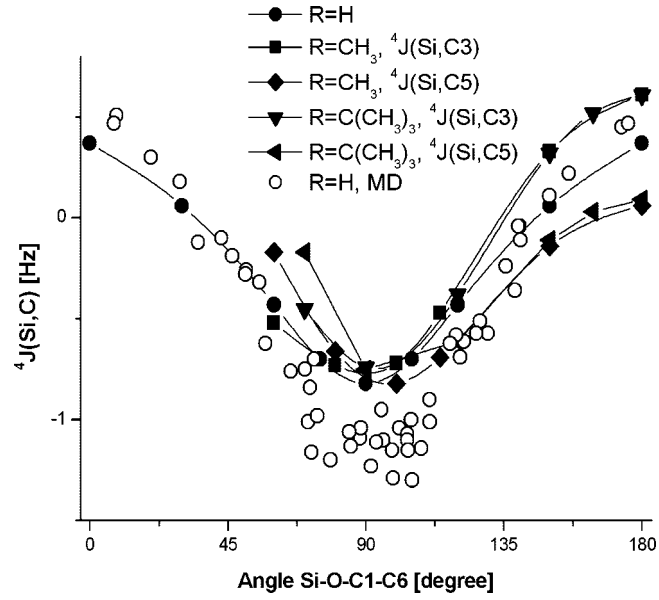


**Figure 7.** The dependence of the $^4J$(Si,C) couplings on the rotation of the TMSO group calculated with the B3LYP method including a chloroform solvent.

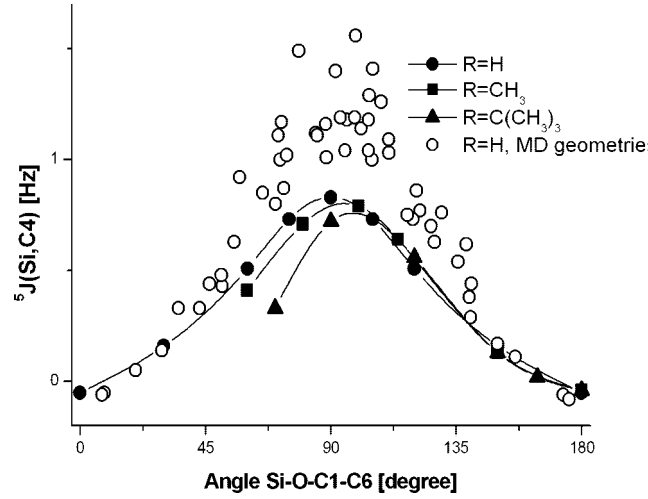


**Figure 8.** The dependence of the $^5J$(Si,C) couplings on the rotation of the TMSO group calculated with the B3LYP method including a chloroform solvent.

vibrational states $n$ (B3LYP) and $m$ (MP2) ($\langle J\rangle_{n,m}$) and the thermal average of the couplings ($\langle J\rangle_{293K}$) (Figure 9; Table 1). The $\langle J\rangle_{n,m}$ values change rather dramatically, and their "quantum character" manifests itself particularly in the case of the low-lying rotational states (Figure 9). The discontinuity of the average couplings $\langle J\rangle_{n,m}$ (Figure 9; B3LYP) corresponds to the alternation of the localization of the states between the global and local minima (Figure 4; B3LYP). With the increase of activation energy, the internal rotation states become delocalized, which leads to merging of both alternating dependencies (for the states with $n > 50$; Figure 9; B3LYP). A similar strong modulation of the average couplings was calculated for the MP2 model potential; however, the delocalization of the rotational states (narrowing of the dependence) corresponded to a higher activation energy (for the states with $m > 120$; Figure 9).

The average couplings $\langle J\rangle_{n,m}$ shown in Table 1 correspond to completely delocalized internal rotation states. Of course, the individual rotational states cannot be probed by the NMR experiment as they cannot be selectively populated in the thermal bath of the liquid-state experiment. The thermal averages are more reliable quantities for comparisons (eq 3 in the Dynamical Calculations subsection). It should be emphasized, however, that a physically correct approach would require a complete accounting of the role of all molecular motions.

The absolute difference between the $\langle J\rangle_{293K}$ couplings and the couplings calculated using the static approach ranges from 0.9 ($^3J$(Si,C2); R = H; B3LYP) to 0.0 Hz ($^2J$(Si,C1); R = $C(CH_3)_3$; B3LYP, MP2). The absolute difference between the $\langle J\rangle$ couplings and experiment ranges from 0.8 ($^3J$(Si,C2); R = H; B3LYP) to 0.0 Hz ($^5J$(Si,C4); R = H; B3LYP). The overall average relative deviation from experiment in percents ($(100/N)_{i=1,\ldots,N}\,|(J_i^{exp} - J_i^{cal})/J_i^{exp}|$), taking all $N$ couplings ($^nJ$, $n = 2$, 3, 4, 5; R = H, R = $CH_3$, R = $C(CH_3)_3$) calculated for the static approach into consideration, was 84 (B3LYP) and 54% (MP2), whereas in the case of the thermal average, it was 46 (B3LYP) and 37% (MP2).

The scalar couplings modeled with the classical MD geometry (54 snap shots) were calculated only for the R = H substitution

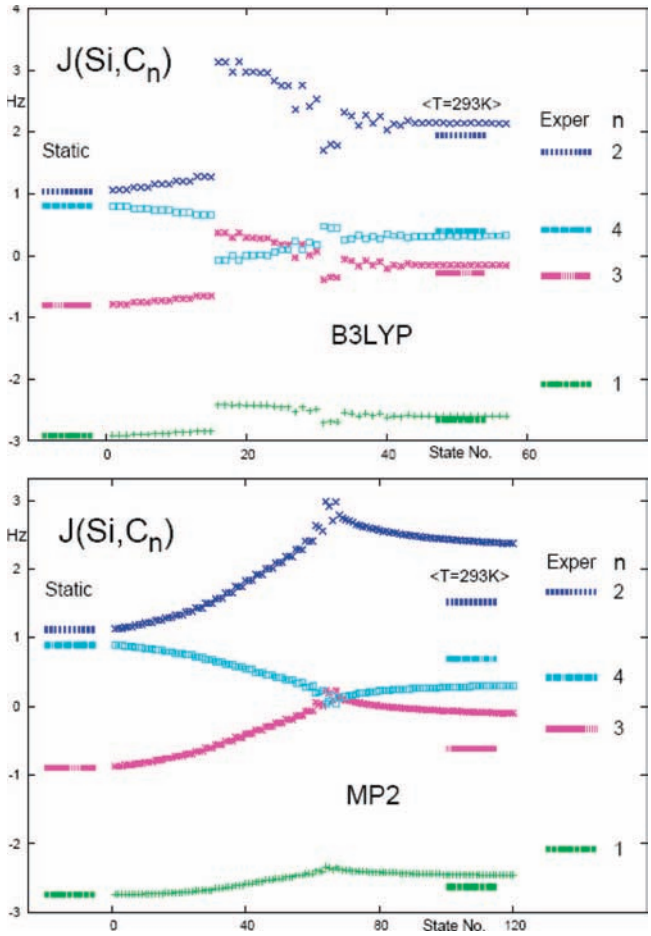


**Figure 9.** The static (equilibrium geometry), vibrational (eq 2 in the Dynamical Calculations subsection), thermal average (eq 3 in the Dynamical Calculations subsection; $T = 293$ K), and the experimental values of the spin−spin coupling constants calculated with the B3LYP and MP2 rotation potential including a chloroform solvent.

(Figures 5–8). The dispersion of the calculated couplings is large when they are correlated only with torsion $\tau$ as all the vibrational modes are active in the MD simulation. Interestingly, this "complete" vibrational effect decreases with the number of bonds between the coupled nuclei increasing. The dispersion of the MD couplings arising due to molecular vibrations is smoothed out, and the MD couplings fit relatively well to the B3LYP calculations (Figures 5–8). The $^2J$(Si,C1) couplings calculated with MD geometries are larger than those calculated with the B3LYP method (Figure 5). This systematic deviation can most probably be attributed to the drawbacks of the used force field. The overall difference of the MD couplings from experiment is larger than the difference obtained with the static and dynamic approach (R = H; Table 1). On the other hand, the MD approach is more advantageous when compared to the quantum approach because it allows for the simultaneous treatment of all molecular vibrational modes. However, a better adjustment of the force field parameters in that regard seems to be necessary.

## Conclusion

The scalar coupling constants for the silicon nucleus of the TMSO group and the carbon nuclei of the phenyl ring were theoretically modeled and measured.

The degree of the internal rotation flexibility was probed for the TMSO group in the three silylated phenols, and the theoretical method for the calculation of the scalar couplings including rotational motion was found to be superior to the approach that uses only static geometry.

A decrease in the rotation flexibility of the TMSO group with the size of the substituent (−H, $-CH_3$, $-C(CH_3)_3$) in the *ortho* position of the phenyl ring was found using the B3LYP and MP2 methods including the effect of environment (gas phase, chloroform − actual experiment, water).

The potential energy surfaces calculated for the TMSO rotation differ for the B3LYP and MP2 methods. For the −H substitutent, the geometry of the local energy minima calculated with the B3LYP method corresponds to the transition state calculated with the MP2 method, and the MP2 internal rotation barrier is roughly four times higher than the B3LYP barrier. The larger substituent groups ($-CH_3$, $-C(CH_3)_3$) effectively hinder the rotation of the TMSO group (steric clash), and the optimal value of the internal rotation coordinate progressively shifts toward the antiperiplanar orientation.

The effect of the environment (gas phase, chloroform, water) on the internal rotational potential is smaller than the calculation method effects (B3LYP, MP2). For arrangements of the TMSO group which are out of the steric clash region, the inclusion of solvent (chloroform, water) leads to an increase in the energy of the internal rotational potential as compared to the gas phase. An opposite trend is found for the structures within the steric clash region.

For the static approach, the overall average deviation of the calculated scalar couplings from experiment was 84 and 54% for the B3LYP and MP2 methods, respectively.

The quality of the internal rotational potential substantially affects the calculated averages of the scalar couplings. The overall average deviation of the calculated thermally averaged scalar couplings from experiment decreases, when compared to the static approach, to 46 and 37% for the B3LYP and MP2 methods, respectively.

Better overall agreement of both static and rotationally averaged scalar couplings with the experiment obtained with the MP2 internal rotation potential is in agreement with the CCSD calculations that indicate a similar internal rotational barrier of the free rotation as a barrier calculated with the MP2 method.

The theoretical models presented in this work strongly indicate that the inclusion of the molecular dynamics is necessary for an accurate calculation of the scalar coupling constants and their reliable structural interpretation if the spin−spin coupling pathway includes atoms that possess large-amplitude molecular motions.

**Acknowledgment.** This work was supported by the Grant Agency of the ASCR (Grant No. IAA A400550701, A400550702, and 400720706) and the Czech Science Foundation (Grant No. 203/06/0738) and by Grant No. LC512 from the Ministry of Education, Youth and Sports of the Czech Republic. This work was a part of the Research Project Z40550506.

**Supporting Information Available:** Additional parameters. This material is available free of charge via the Internet at http://pubs.acs.org.

## References and Notes

(1) Grant, D. M.; Harris, R. K. *Encyclopedia of Nuclear Magnetic Resonance*; Wiley: Sussex, U.K., 1996.
(2) Karplus, M. *J. Chem. Phys.* **1959**, *30*, 11.
(3) Altona, C.; Sundaral, M. *J. Am. Chem. Soc.* **1973**, *95*, 2333.
(4) Davies, D. B. *Prog. Nucl. Magn. Reson. Spectrosc.* **1978**, *12*, 135.

(5) Pardi, A.; Wagner, G.; Wüthrich, K. *Eur. J. Biochem.* **1983**, *137*, 445.
(6) Pardi, A.; Billeter, M.; Wüthrich, K. *J. Mol. Biol.* **1984**, *180*, 741.
(7) Smith, L. J.; Bolin, K. A.; Schwalbe, H.; MacArthur, M. W.; Thornton, J. M.; Dobson, C. M. *J. Mol. Biol.* **1996**, *255*, 494.
(8) Bühl, M.; Imhof, P.; Repisky, M. *ChemPhysChem* **2004**, *5*, 410.
(9) Jordan, M. J. T.; Toh, J. S. S.; Del Bene, J. E. *Chem. Phys. Lett.* **2001**, *346*, 288.
(10) Del Bene, J. E.; Jordan, M. J. T. *J. Phys. Chem. A* **2002**, *106*, 5385.
(11) Ruden, T. A.; Helgaker, T.; Jaszunski, M. *Chem. Phys.* **2004**, *296*, 53.
(12) Ruden, T. A.; Lutnaes, O. B.; Helgaker, T.; Ruud, K. *J. Chem. Phys.* **2003**, *118*, 9572.
(13) Kaupp, M.; Bühl, M.; Malkin, V. *Calculation of NMR and EPR Parameters*; Willey-VCH Verlag: Weinheim, Germany, 2004.
(14) Becke, A. D. *J. Chem. Phys.* **1993**, *98*, 5648.
(15) Frisch, M. J.; Headgordon, M.; Pople, J. A. *Chem. Phys. Lett.* **1990**, *166*, 275.
(16) Cizek, J. *J. Chem. Phys.* **1966**, *45*, 4256.
(17) Purvis, G. D.; Bartlett, R. J. *J. Chem. Phys.* **1982**, *76*, 1910.
(18) Hariharan, P. C.; Pople, J. A. *Theor. Chim. Acta* **1973**, *28*, 213.
(19) Francl, M. M.; Pietro, W. J.; Hehre, W. J.; Binkley, J. S.; Gordon, M. S.; Defrees, D. J.; Pople, J. A. *J. Chem. Phys.* **1982**, *77*, 3654.
(20) Cammi, R.; Mennucci, B.; Tomasi, J. *J. Phys. Chem. A* **2000**, *104*, 5631.
(21) Frisch, M. J. Trucks, G. W.; Schlegel, H. B.; Scuseria, G. E.; Robb, M. A.; Cheeseman, J. R.; Montgomery, J. A.; Jr Vreven, T.; Kudin, K. N.; Burant, J. C.; Millam, J. M.; Iyengar, S. S.; Tomasi, J.; Barone, V.; Mennucci, B.; Cossi, M.; Scalmani, G.; Rega, N.; Petersson, G. A.; Nakatsuji, H.; Hada, M.; Ehara, M.; Toyota, K.; Fukuda, R.; Hasegawa, J.; Ishida, M.; Nakajima, T.; Honda, Y.; Kitao, O.; Nakai, H.; Klene, M.; Li, X.; Knox, J. E.; Hratchian, H. P.; Cross, J. B.; Bakken, V.; Adamo, C.; Jaramillo, J.; Gomperts, R.; Stratmann, R. E.; Yazyev, O.; Austin, A. J.; Cammi, R.; Pomelli, C.; Ochterski, J. W.; Ayala, P. Y.; Morokuma, K.; Voth, G. A.; Salvador, P.; Dannenberg, J. J.; Zakrzewski, V. G.; Dapprich, S.; Daniels, A. D.; Strain, M. C.; Farkas, O.; Malick, D. K.; Rabuck, A. D.; Raghavachari, K.; Foresman, J. B.; Ortiz, J. V.; Cui, Q.; Baboul, A. G.; Clifford, S.; Cioslowski, J.; Stefanov, B. B.; Liu, G.; Liashenko, A.; Piskorz, P.; Komaromi, I.; Martin, R. L.; Fox, D. J.; Keith, T.; Al-Laham, M. A.; Peng, C. Y.; Nanayakkara, A.; Challacombe, M.; Gill, P. M. W.; Johnson, B.; Chen, W.; Wong, M. W.; Gonzalez, C.; Pople, J. A. *Gaussian 03*, revision C.02; Gaussian, Inc.: Wallingford, CT, 2004.
(22) Helgaker, T.; Jaszunski, M.; Ruud, K. *Chem. Rev.* **1999**, *99*, 293.
(23) Sychrovský, V.; Grafenstein, J.; Cremer, D. *J. Chem. Phys.* **2000**, *113*, 3530.
(24) Helgaker, T.; Watson, M.; Handy, N. C. *J. Chem. Phys.* **2000**, *113*, 9402.
(25) Kutzelnigg, W.; Fleischer, U.; Schindler, M. *NMR−Basic Principles and Progress*; Springer: Heidelberg, Germany, 1990.
(26) Hougen, J. T.; Bunker, P. R.; Johns, J. W. C. *J. Mol. Spectrosc.* **1970**, *34*, 136.
(27) Špirko, V.; Kraemer, W. P.; Cejchan, A. *J. Mol. Spectrosc.* **1989**, *136*, 340.
(28) Špirko, V.; Blabla, J. *J. Mol. Spectrosc.* **1988**, *129*, 59.
(29) Sauer, S. P. A.; Moller, C. K.; Koch, H.; Paidarová, I.; Špirko, V. *Chem. Phys.* **1998**, *238*, 385.
(30) Chalupsky, J.; Vondrasek, J.; Špirko, V. *J. Phys. Chem. A* **2008**, *112*, 693.
(31) Vacek, J.; Michl, J. *New J. Chem.* **1997**, *21*, 1259.
(32) Rappe, A. K.; Casewit, C. J.; Colwell, K. S.; Goddard, W. A.; Skiff, W. M. *J. Am. Chem. Soc.* **1992**, *114*, 10024.
(33) Schraml, J.; Hetflejš, J.; Blechta, V.; Šabata, S.; Soukupová, L. *Magn. Reson. Chem.* To be published.
(34) Schraml, J. *Collect. Czech. Chem. Commun.* **1983**, *48*, 3402.
(35) Blechta, V.; Sýkora, J.; Schraml, J. *Magn. Reson. Chem.* **2004**, *42*, 968.
(36) Morris, G. A.; Freeman, R. *J. Am. Chem. Soc.* **1979**, *101*, 760.
(37) Shields, A. E.; van Mourik, T. *J. Phys. Chem. A* **2007**, *111*, 13272.
(38) Kristyan, S.; Pulay, P. *Chem. Phys. Lett.* **1994**, *229*, 175.
(39) Hobza, P.; Sponer, J.; Reschel, T. *J. Comput. Chem.* **1995**, *16*, 1315.
(40) van Mourik, T. *Phys. Chem. Chem. Phys.* **2004**, *6*, 2827.

JP711809E